PAPER

Production of hydrogen peroxide as a sustainable solar fuel from water and dioxygen†

Satoshi Kato,[a] Jieun Jung,[a] Tomoyoshi Suenobu[a] and Shunichi Fukuzumi*[ab]

Hydrogen peroxide was produced as a solar fuel from water and dioxygen using solar energy by combination of a water oxidation catalyst and a photocatalyst for two-electron reduction of O_2 in acidic aqueous solutions. Photocatalytic production of H_2O_2 occurred under photoirradiation of $[Ru^{II}(Me_2phen)_3]^{2+}$ (Me_2phen = 4,7-dimethyl-1,10-phenanthroline) used as a photocatalyst with visible light in the presence of $Ir(OH)_3$ acting as a water oxidation catalyst in an O_2-saturated H_2SO_4 aqueous solution. Photoinduced electron transfer from the excited state of $[Ru^{II}(Me_2phen)_3]^{2+}$ to O_2 results in the formation of $[Ru^{III}(Me_2phen)_3]^{3+}$ and a superoxide radical anion (O_2^{-}) which is protonated to produce H_2O_2 *via* disproportionation of $HO_2^·$ in competition with back electron transfer (BET) from O_2^{-} to $[Ru^{III}(Me_2phen)_3]^{3+}$. $[Ru^{III}(Me_2phen)_3]^{3+}$ oxidises water with the aid of catalysis of $Ir(OH)_3$ to produce O_2. The photocatalytic reactivity of H_2O_2 production was improved by replacing $Ir(OH)_3$ nanoparticles by $[Co^{III}(Cp^*)(bpy)(H_2O)]^{2+}$ in the presence of $Sc(NO_3)_3$ in water. The optimised quantum yield of the photocatalytic H_2O_2 production at λ = 450 nm was determined using a ferrioxalate actinometer to be 37%. The value of conversion efficiency from solar energy to chemical energy was also determined to be 0.25%.

Broader context

Photocatalytic production of hydrogen peroxide from earth-abundant water and dioxygen using solar energy as an ideally sustainable solar fuel has remained a great challenge. We report herein for the first time photocatalytic production of hydrogen peroxide from water and dioxygen under visible light using $[Ru^{II}(Me_2phen)_3]^{2+}$ (Me_2phen = 4,7-dimethyl-1,10-phenanthroline) as a photocatalyst and $Ir(OH)_3$ nanoparticles or $[Co^{III}(Cp^*)(bpy)(H_2O)]^{2+}$ (Cp^* = η^5-pentamethylcyclopentadienyl, bpy = 2,2-bipyridine) as a water oxidation catalyst in water containing H_2SO_4 or $Sc(NO_3)_3$. A high turnover number and quantum yield have been attained by combining an efficient water oxidation catalyst with a photosensitiser and a Lewis acid in water.

1. Introduction

Renewable and clean energy resources are urgently required in order to solve global energy and environmental issues.[1,2] Among renewable energy resources, solar energy is by far the largest exploitable resource,[1–6] and thereby it is quite important to obtain sustainable solar fuels such as hydrogen (H_2) or others. Hydrogen is a clean energy source to reduce the dependence on fossil fuels and the emissions of greenhouse gases in the long term.[7–17] However, the storage of hydrogen has been very difficult, because hydrogen is a gas having a low volumetric energy density.[18,19] In contrast to hydrogen, hydrogen peroxide (H_2O_2),

soluble in water, can be an ideal energy carrier alternative to oil or hydrogen, because it can be used in a one-compartment fuel cell leading to the generation of electricity.[20–27] The output potential of H_2O_2 fuel cells theoretically achievable is 1.09 V, which is somewhat smaller but comparable to those of a hydrogen fuel cell (1.23 V) and a direct methanol fuel cell (1.21 V).[22–27] Thus, a combination of hydrogen peroxide production using solar energy and power generation with a hydrogen peroxide fuel cell provides an ideally sustainable solar fuel.[22] However, photocatalytic production of hydrogen peroxide from water (H_2O) and dioxygen (O_2) using solar energy has remained a great challenge.

H_2O_2 is currently manufactured in industry by the autoxidation of 2-alkyl anthrahydroquinone by O_2 to the corresponding 2-alkylanthraquinone (the so-called anthraquinone process) using a noble metal such as palladium to regenerate the anthrahydroquinone with H_2.[28] H_2 used as a reductant is normally produced by steam reforming of natural gases, which emits a significant amount of CO_2.[28] H_2O_2 can also be produced by two-electron photoreduction of O_2 with use of a

[a]Department of Material and Life Science, Division of Advanced Science and Biotechnology, Graduate School of Engineering, Osaka University, ALCA, Japan Science and Technology Agency (JST), Suita, Osaka 565-0871, Japan. E-mail: fukuzumi@chem.eng.osaka-u.ac.jp; Fax: +81-6-6879-7370; Tel: +81-6-6879-7368

[b]Department of Bioinspired Science, Ewha Womans University, Seoul 120-750, Korea. E-mail: wnnam@ewha.ac.kr

† Electronic supplementary information (ESI) available: Experimental details and additional data. See DOI: 10.1039/c3ee42815j

semiconductor photocatalyst[29] or a homogeneous photo-catalyst.[30–33] In this case, organic reductants such as 2-propanol, acetaldehyde and oxalate are required as sacrificial electron sources, resulting in unwanted emission of CO_2.[29–33]

We report herein for the first time photocatalytic production of H_2O_2 from H_2O and O_2, both of which are earth abundant, without emission of CO_2 by two-electron photoreduction of O_2 by H_2O that is used as an electron source in acidic aqueous solutions. The high turnover number and quantum yield have been attained by combining an efficient water oxidation catalyst (WOC) with a photosensitiser and a scandium ion that acts as a Lewis acid and facilitates two-electron reduction of O_2. The present study will pave a way to utilise H_2O_2 produced from H_2O and O_2 as a sustainable solar fuel in an H_2O_2 fuel cell.[22]

2. Experimental section

2.1 Materials

All chemicals commercially available were used without further purification unless otherwise noted. $H_2IrCl_6 \cdot 5.5H_2O$ (99.99%) and IrO_2 (99%) were purchased from Furuya Metal. $RuCl_3 \cdot 3H_2O$ (38.220 wt% Ru) was purchased from Tanaka Kikinzoku Kogyo K.K. 4,7-Dimethyl-1,10-phenanthroline (Me$_2$phen, 98%), tris(2,2′-bipyridyl)ruthenium(II) dichloride hexahydrate ([Ru^{II}(bpy)$_3$]Cl$_2 \cdot 6H_2O$), *tert*-butyllithium (1.7 M in *n*-pentane), Ag_2SO_4 (99.9%), $(NH_4)_2SO_4$ (99.99%), *n*-pentane, $Y(NO_3)_3 \cdot 4H_2O$ (99.99%), $Lu(NO_3)_3 \cdot nH_2O$ (99.999%) and $Mg(NO_3)_2 \cdot 6H_2O$ (99.999%) were supplied by Aldrich Chemicals. MnO_2 (85%), $CoCl_2$ (95.0%), 2,2′-bipyridine (bpy, 99.0%), tetrahydrofuran and $Ca(NO_3)_2 \cdot 4H_2O$ (99.9%) were purchased from Wako Pure Chemical Industries Ltd. Pentamethylcyclopentadiene was obtained from Kanto Chemical Co., Inc. Oxo[5,10,15,20-tetra(4-pyridyl)porphinato]titanium(IV) ([TiO(tpyp)]) was supplied by Tokyo Chemical Industry Co., Ltd. (TCI). $Sc(NO_3)_3 \cdot 4H_2O$ (99.9%) was supplied by Mitsuwa Chemicals Co., Ltd. PbO_2 (90%) and $Zn(NO_3)_2 \cdot 6H_2O$ (99%) were supplied by Nacalai Tesque. $^{18}O^{18}O$ gas (≥98 at.%) was purchased from TAIYO NIPPON SANSO Corporation as a compressed gas in a cylinder (0.5 L). Carbon monoxide (CO) gas was purchased from Sumitomo Seika Chemicals Co., Ltd. as a compressed gas in a cylinder (3.4 L). Purification of water (18.2 MΩ cm) was performed with a Milli-Q system (Millipore, Direct-Q 3 UV).

2.2 Synthesis of iridium hydroxide nanoparticles

Iridium hydroxide nanoparticles were synthesised according to the literature.[34] The pH of an aqueous solution of H_2IrCl_6 was adjusted to ~10 by adding 5.0 M NaOH solution with vigorous stirring at 100 °C. After 1.0 h stirring, precipitates appeared were collected by centrifugation. Then, the precipitates were washed by water three times, dried *in vacuo* at room temperature and kept at 65 °C for 10 h.

2.3 Synthesis of [Ru^{II}(Me$_2$phen)$_3$]SO$_4$

The tris(4,7-dimethyl-1,10-phenanthroline)ruthenium(II) sulphate ([Ru^{II}(Me$_2$phen)$_3$]SO$_4$) complex was synthesised according to the literature.[35] $RuCl_3$ was refluxed under N_2 overnight in ethanol–water (v/v 80/20) with 6 equiv. of ligand, Me$_2$phen, to form the red-orange [Ru^{II}(Me$_2$phen)$_3$]Cl$_2$ complex. After evaporation of the solvent, the product was readily precipitated from acetone with ether. The precipitate, [Ru^{II}-(Me$_2$phen)$_3$]Cl$_2$, was added to water to be completely dissolved and Ag_2SO_4 (65 mg) solubilised in water was added to the solution. After stirring for 12 h, AgCl was filtered off as a precipitate. An aqueous solution of $(NH_4)_2SO_4$ was added to the reaction solution to obtain a crystalline product.

2.4 Synthesis of [Co(Cp*)(bpy)(OH$_2$)]SO$_4$

The [Co(Cp*)(bpy)(OH$_2$)]SO$_4$ complex was synthesised according to the literature.[36] Pentamethylcyclopentadiene (Cp*, 25 mL) and *tert*-butyllithium (~1.7 M in *n*-pentane, 90 mL) were combined in an equimolar amount (1 : 1) in *n*-pentane at 203 K. The solution was stirred and slowly allowed to warm up to room temperature. After stirring for further 24 h at room temperature, a white suspension was filtered through an inert gas frit and pentamethylcyclopentadienyllithium (Cp*Li) was filtered off. The anhydrous $CoCl_2$ (1.32 g) was added to the solution of Cp*Li (1.42 g) in 20 mL of tetrahydrofuran. The mixture was stirred for 3 h at room temperature until the brown solution became green-brown. Afterwards the solution was concentrated to a smaller volume under reduced pressure and extracted with 100 mL of *n*-pentane. The brown extracts were bubbled by CO gas for 30 min through the solution. Di-μ-chloro-bis[chloro-(η^5-pentamethylcyclopentadienyl)cobalt] ([(μ-Cl)(CoCp*Cl)]$_2$) was obtained as a green powder. The [(μ-Cl)(CoCp*Cl)]$_2$ (100 mg) in 20 mL of water was stirred with 1.5 equimolar amount of 2,2′-bipyridine (88 mg) for 1 h at room temperature under N_2. After filtering off free 2,2′-bipyridine, Ag_2SO_4 (118 mg) was added to the filtrate. After stirring for 12 h, AgCl was filtered off as a precipitate. An aqueous solution of $(NH_4)_2SO_4$ was added to the reaction solution to obtain a crystalline product. ^{1}H-NMR (300 MHz, D$_2$O): δ (ppm) = 1.34 (s, 15H), 8.10 (t, J = 5.86 Hz, 2H), 8.43 (t, J = 8.06 Hz, 2H), 8.51 (d, J = 8.06 Hz, 2H), 9.85 (d, J = 5.50 Hz, 2H).

2.5 Quantum yield and quantum efficiency measurements

The quantum yield (QY) of the photocatalytic production of hydrogen peroxide (Φ) was determined under irradiation of monochromatised light using a Shimadzu spectrofluorophotometer (RF-5300PC) through a band-pass filter transmitting λ = 450 nm, and estimated as

$$QY \, (\%) = (2 \times R/I) \times 100 \tag{1}$$

where R (mol s^{-1}) represents the H_2O_2 production rate and I coefficient (Einstein s^{-1}) based on the rate of the number of incident photons. In order to produce hydrogen peroxide by two-electron reduction of one molecule of oxygen, two photons are necessary for the electronic transition of the [Ru^{II}(Me$_2$phen)$_3$]$^{2+}$ photosensitiser. When the total two photons are fully used for production of hydrogen peroxide, QY reaches 100%. Therefore, the coefficient of the right-hand side in eqn (1) is 2 for this photocatalytic system. The total number of incident

This journal is © The Royal Society of Chemistry 2013

Energy Environ. Sci., 2013, **6**, 3756–3764 | 3757

photons was measured by a standard method using an actinometer (potassium ferrioxalate, $K_3[Fe^{III}(C_2O_4)_3]$[37] in H_2O at room temperature under photoirradiation of a Shimadzu spectrofluorophotometer (RF-5300PC) through a band-pass filter transmitting $\lambda = 450$ nm (slit width of 5.0 mm) at room temperature. For the same quartz cuvette (light path length = 1 cm) with 3.0 mL solution as used in the production of hydrogen peroxide experiments, the rate of photon flux of the incident light (I) was determined to be 1.11×10^{-9} Einstein s^{-1}. $Ir(OH)_3$ (3.0 mg) or $[Co^{III}(Cp^*)(bpy)(H_2O)]SO_4$ (10 mM) was added to an H_2SO_4 aqueous solution (2.0 M, 3.0 mL) containing $[Ru^{II}(Me_2phen)_3]SO_4$ (20 μM) or to distilled water (3.0 mL) containing $[Ru^{II}(Me_2phen)_3]SO_4$ (20 μM) and $Sc(NO_3)_3$ (100 mM) in a quartz cuvette (light path length = 1 cm). The solution was saturated by bubbling with oxygen gas for ~30 min. The photocatalyst was irradiated with a Shimadzu spectrofluorophotometer (RF-5300PC) through a band-pass filter transmitting $\lambda = 450$ nm (slit width of 5.0 mm) at room temperature. The amount of produced hydrogen peroxide was determined by spectroscopic titration with an acidic solution of the $[TiO(tpypH_4)]^{4+}$ complex (Ti-TPyP reagent).[38] The Ti-TPyP reagent was prepared by dissolving 34.03 mg of the $[TiO(tpyp)]$ complex in 1000 mL of 50 mM hydrochloric acid. A small portion (100 μL) of the reaction solution was sampled and diluted with water. To 0.25 mL of the diluted sample, 0.25 mL of 4.8 M perchloric acid and 0.25 mL of the Ti-TPyP reagent were added. The mixed solution was then allowed to stand for 5 min at room temperature. This sample solution was diluted to 2.5 mL with water and used for the spectroscopic measurement. The absorbance at $\lambda = 434$ nm was measured using a Hewlett Packard 8453 diode array spectrophotometer (A_S). A blank solution was prepared in a similar manner by adding distilled water instead of the sample solution in the same volume with its absorbance designated as A_B. The difference in absorbance was determined as follows: $\Delta A_{434} = A_B - A_S$. Based on ΔA_{434} and the volume of the solution, the amount of hydrogen peroxide was determined according to the literature.[38]

2.6 Measurements of conversion efficiency from solar energy

Typically, $[Co^{III}(Cp^*)(bpy)(H_2O)]SO_4$ (10 mM) was added to distilled water (3.0 mL) containing $[Ru^{II}(Me_2phen)_3]SO_4$ (100 μM) and $Sc(NO_3)_3$ (100 mM) in a quartz cuvette (light path length = 1 cm). The solution was saturated by bubbling with oxygen gas for ~30 min. The photocatalyst was irradiated with a solar simulator (HAL-320, Asahi Spectra Co., Ltd.). The light intensity was adjusted to be 10 mJ cm^{-2} s^{-1} (Air Mass 1.5 (AM1.5)) at the sample position for the whole irradiation area (1.0×3.0 cm^2) using a 1 SUN checker (CS-20, Asahi Spectra Co., Ltd.) at room temperature. The amount of produced hydrogen peroxide was determined by the titration with the Ti-TPyP reagent (*vide supra*).

2.7 Spectral measurements

Typically, an H_2SO_4 aqueous solution (2.0 M, 3.0 mL) containing $[Ru^{II}(Me_2phen)_3]SO_4$ (20 μM) in a quartz cuvette (light path length = 1 cm) was saturated with O_2 by bubbling with oxygen

gas for ~30 min. The photocatalysts were irradiated with a Shimadzu spectrofluorophotometer (RF-5300PC) at $\lambda = 450$ nm with a slit width of 5.0 mm at room temperature. The generation of $[Ru^{III}(Me_2phen)_3]^{3+}$ was monitored by the decrease of the absorption band at $\lambda = 445$ nm due to $[Ru^{II}(Me_2phen)_3]^{2+}$ ($\varepsilon = 2.5 \times 10^4$ M^{-1} cm^{-1})[39] as well as the increase in the absorption band at $\lambda = 630$ nm due to $[Ru^{III}(Me_2phen)_3]^{3+}$ ($\varepsilon = 1.6 \times 10^3$ M^{-1} cm^{-1}) using a Hewlett Packard 8453 diode array spectrophotometer.

2.8 Isotope-labelling experiments

$Ir(OH)_3$ (3.0 mg) was dispersed in an H_2SO_4 aqueous solution (2.0 M, 3.0 mL) containing $[Ru^{II}(Me_2phen)_3]SO_4$ (20 μM) in a quartz cuvette (light path length = 1 cm). The solution was saturated by bubbling with $^{18}O^{18}O$ gas. The solution was irradiated with a xenon lamp (USHIO Optical Modulex SX-UID 501XAMQ) through a cut-off filter (Asahi Techno Glass L42) transmitting $\lambda > 420$ nm at room temperature. After 3 h, the solution was deaerated by bubbling with He gas for ~30 min to exclude the $^{18}O^{18}O$ gas. At 10 min after addition of an excess amount of manganese oxide (MnO_2) to the solution, 50 mL of the gas in a headspace was sampled using a gas-tight syringe for gas analysis. The ratio of $^{16}O^{16}O$, $^{16}O^{18}O$ and $^{18}O^{18}O$ was determined based on the intensity of mass spectra ($m/z = 32$, 34 and 36) obtained using a Shimadzu GC-17A gas chromatograph [He carrier, TC-FFAP column (GL Science, 1010-15242) at 313 K] equipped with a mass spectrometer (Shimadzu, QP-5000).

2.9 EPR measurements

The EPR spectrum was taken on a JEOL X-band spectrometer (JES-RE1XE) under nonsaturating microwave power conditions (1.0 mW) operating at 9.2 GHz. Distilled water (1.0 mL) containing $[Ru^{II}(Me_2phen)_3]SO_4$ (20 μM) and $Sc(NO_3)_3$ (100 mM) in the EPR tube was saturated by bubbling with pure O_2 for ~30 min. The solution was frozen at 77 K after visible light irradiation ($\lambda > 420$ nm). The magnitude of the modulation was chosen to optimise the resolution and the signal to noise ratio (S/N) of the observed spectrum (modulation width, 2.0 G; modulation frequency, 100 kHz). The g values were calibrated using an Mn^{2+} marker.

2.10 Characterisation of $Ir(OH)_3$ nanoparticles

X-ray photoelectron spectra (XPS) were recorded using a Kratos Axis 165 with a 165 mm hemispherical electron energy analyser. The incident radiation was Mg Kα X-ray (1253.6 eV) at 200 W and a charge neutraliser was turned on for acquisition. Each sample was attached on a stainless stage with a double-sided carbon scotch tape. The binding energy of each element was corrected by the C 1s peak (284.6 eV) from residual carbon. TG/DTA data were recorded on an SII TG/DTA 7200 instrument. Each sample (~3.0 mg) was heated from 298 K to 373 K (held at 373 K for 10 min) and from 373 K to 873 K with a ramp rate of 2 K min^{-1}. A certain amount of γ-Al_2O_3 was used as a reference for DTA measurements. Nitrogen adsorption–desorption at 77 K was performed with a Belsorp-mini (BEL Japan, Inc.) within a relative pressure range from 0.01 to 101.3 kPa. A sample mass

3758 | *Energy Environ. Sci.*, 2013, **6**, 3756–3764

This journal is © The Royal Society of Chemistry 2013

used for adsorption analysis was pretreated at 333 K for 30 min under vacuum conditions and kept in a N_2 atmosphere until N_2-adsorption measurements. The sample was exposed to a mixed gas of He and N_2 with a programmed ratio and the adsorbed amount of N_2 was calculated from the change of pressure in a cell after reaching equilibrium (at least 5 min). The transmission electron microscopy (TEM) image of iridium hydroxide, which was mounted on a copper microgrid coated with elastic carbon, was observed using a JEOL JEM-2100 operating at 200 keV.

3. Results and discussion

3.1 Characterisation of Ir(OH)$_3$ nanoparticles

The TG curve of Ir(OH)$_3$ nanoparticles is shown in Fig. 1a, which exhibits two consecutive steps. The first step of weight loss with an endothermic peak at 393 K corresponds to the removal of physisorbed water. The weight loss at the second step of Ir(OH)$_3$ starting from 583 K was attributed to dehydration of Ir(OH)$_3$. The TG curve of commercially available IrO$_2$ in Fig. 1b showed no such dehydration step.

To determine surface conditions of Ir(OH)$_3$, X-ray photoelectron spectroscopy (XPS) measurements were carried out for the energy regions of Ir 4f, O 1s and C 1s with reference to commercially available IrO$_2$. As reported previously, the binding energy of Ir 4f$_{5/2}$ reflects the valence of Ir ions sensitively where the binding energies of Ir 4f$_{5/2}$ for Ir^0, Ir^{III} and Ir^{IV} are reported to be 61.0 eV, 62.0 eV and 63.7 eV, respectively.[40–42] The XPS

spectra of Ir 4f and O 1s for the iridium hydroxide and IrO$_2$ are shown in Fig. 2. The binding energy of Ir 4f$_{5/2}$ of both the iridium hydroxide and IrO$_2$ was 62.2 eV, which is close to the reported binding energy of 62.0 eV for Ir(III) species. The O 1s peaks of the iridium hydroxide and IrO$_2$ appeared at 531.5 eV and 530.5 eV, respectively. The higher binding energy of the O 1s peak of the iridium hydroxide results from the formation of hydroxide species as often reported previously.[43,44]

Iridium hydroxide was investigated by transmission electron microscopy (TEM). The TEM image is displayed in Fig. 3, which indicates that the size is in the range of 50–100 nm with an undefined shape. BET surface areas of Ir(OH)$_3$ and IrO$_2$ (commercially available) are shown in Table S1 in the ESI.† The BET surface area of Ir(OH)$_3$ was 28 times higher than that of IrO$_2$.

3.2 Photocatalytic production of H$_2$O$_2$ from H$_2$O and O$_2$ with Ir(OH)$_3$ nanoparticles

Photoexcitation of [Ru^{II}(Me$_2$phen)$_3$]$^{2+}$ (Me$_2$phen = 4,7-dimethyl-1,10-phenanthroline) results in the generation of [Ru^{III}(Me$_2$phen)$_3$]$^{3+}$ by oxidative quenching of the photoexcited state ([Ru^{II}(Me$_2$phen)$_3$]$^{2+}$*: * denotes the excited state) with O$_2$ in the presence of H$_2$SO$_4$ to produce H$_2$O$_2$ as reported for the case of [Ru^{II}(bpy)$_3$]$^{2+}$ (bpy = 2,2′-bipyridine).[45] The time courses of [Ru^{III}(Me$_2$phen)$_3$]$^{3+}$ generation and H$_2$O$_2$ production are shown in Fig. 4. One-half equiv. of H$_2$O$_2$ was produced, accompanied by the formation of [Ru^{III}(Me$_2$phen)$_3$]$^{3+}$ under
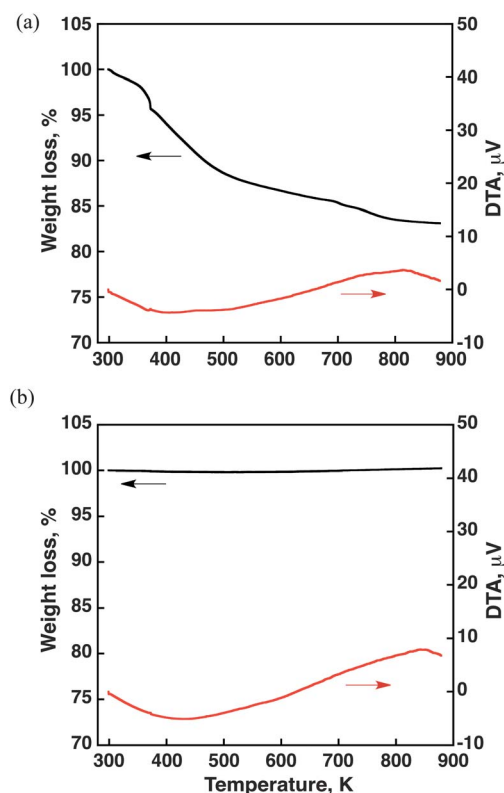
Fig. 1 TG/DTA data for (a) Ir(OH)$_3$ and (b) IrO$_2$ (TG curve: black, DTA curve: red). The temperature increased from 298 K to 873 K with a ramp rate of 2 K min^{-1}.
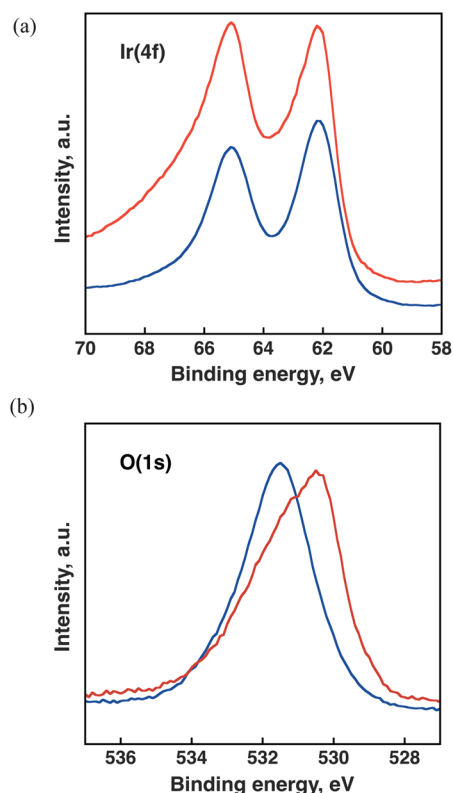
Fig. 2 X-ray photoelectron spectra in the binding energy regions of Ir 4f and O 1s for (a) Ir(OH)$_3$ (blue line) and (b) IrO$_2$ (red line).
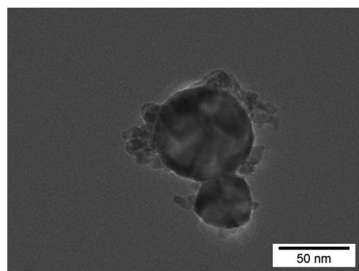
This journal is © The Royal Society of Chemistry 2013

Energy Environ. Sci., 2013, **6**, 3756–3764 | **3759**

Fig. 3 TEM image of Ir(OH)$_3$ nanoparticles.
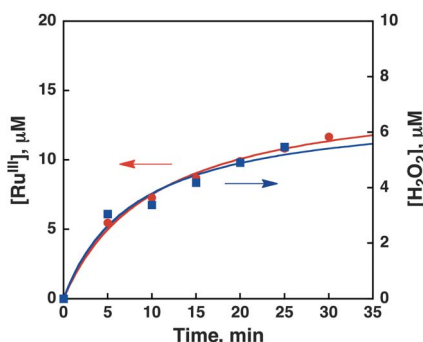
Fig. 4 Time courses of [Ru^{III}(Me$_2$phen)$_3$]$^{3+}$ generation (red line) and H$_2$O$_2$ production (blue line) under irradiation of [Ru^{II}(Me$_2$phen)$_3$]$^{2+}$ (20 μM) with visible light (λ = 450 nm) in an air-saturated H$_2$SO$_4$ aqueous solution (2.0 M, 3.0 mL, [O$_2$] = 0.25 mM).

photoirradiation of [Ru^{II}(Me$_2$phen)$_3$]$^{2+}$ in an air-saturated aqueous solution containing 2.0 M H$_2$SO$_4$. Thus, the stoichiometry of the photochemical reaction is given by eqn (2).

$$2\left[Ru^{II}(Me_2phen)_3\right]^{2+} + O_2 + 2H^+ \xrightarrow{h\nu}$$
$$2\left[Ru^{III}(Me_2phen)_3\right]^{3+} + H_2O_2 \quad (2)$$
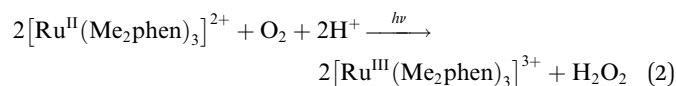
The quantum yield (Φ) of generation of [Ru^{III}(Me$_2$phen)$_3$]$^{3+}$ (21%) at the initial stage (0–1 min) was significantly larger than that of [Ru^{III}(bpy)$_3$]$^{3+}$ (1.6%) in the presence of 2.0 M H$_2$SO$_4$ (Fig. S1 in the ESI†) because the one-electron oxidation potential of [Ru(Me$_2$phen)$_3$]$^{2+*}$ ($E^0_{red}* = -1.01$ V $vs.$ NHE) is more negative than [Ru(bpy)$_3$]$^{2+*}$ ($E^0_{red}* = -0.84$ V $vs.$ NHE).[46] The Φ value at the initial stage (0–1 min) increased with increasing the concentration of H$_2$SO$_4$ to reach 72% in the presence of 4.0 M H$_2$SO$_4$ (Table S2 in the ESI†).

With regard to a water oxidation catalyst (WOC), an efficient but acid-stable catalyst must be used for the photocatalytic production of H$_2$O$_2$ from H$_2$O and O$_2$. Ir(OH)$_3$ nanoparticles[34] are found to be suitable for this purpose. The photocatalytic production of H$_2$O$_2$ from H$_2$O and O$_2$ [eqn (3)] was examined using [Ru^{II}(Me$_2$phen)$_3$]SO$_4$ as a photosensitiser for the two-electron reduction of O$_2$ and Ir(OH)$_3$ nanoparticles as a WOC in an O$_2$-saturated H$_2$SO$_4$ aqueous solution (2.0 M). The sulphate complex was used to avoid possible oxidation of the chloride anion during the photocatalytic water oxidation.

$$2H_2O + O_2 \xrightarrow[\left[Ru^{II}(Me_2phen)_3\right]^{2+}, Ir(OH)_3]{h\nu} 2H_2O_2 \quad (3)$$
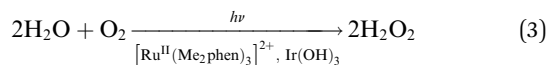
The time courses of H$_2$O$_2$ production in the solution are shown in Fig. 5a. The turnover number (TON) based on [Ru^{II}(Me$_2$phen)$_3$]$^{2+}$ was determined to be 307 after 18 h photo-irradiation. No H$_2$O$_2$ production was observed from a reaction solution without [Ru^{II}(Me$_2$phen)$_3$]$^{2+}$. The photocatalytic reactivity increased with increasing the concentration of H$_2$SO$_4$ and exhibits a maximum value at 2.0 M H$_2$SO$_4$ (Fig. S2 in the ESI†). At H$_2$SO$_4$ concentrations higher than 2.0 M, the catalytic reactivity of Ir(OH)$_3$ nanoparticles decreased because Ir(OH)$_3$ nanoparticles became partially dissolved under strongly acidic conditions. Ir(OH)$_3$ nanoparticles were clearly dissolved in water with 3.0 M H$_2$SO$_4$. The photocatalytic reactivity increased with increasing the amount of Ir(OH)$_3$ nanoparticles, but it decreased through a maximum value with further increase in the amount of Ir(OH)$_3$ (Fig. 5b) because of the competition of the visible light absorption of [Ru^{II}(Me$_2$phen)$_3$]$^{2+}$ with that of Ir(OH)$_3$ nanoparticles. The Φ value of the photocatalytic H$_2$O$_2$ production at λ = 450 nm was determined using a ferrioxalate actinometer to be 20% (0–30 min, Fig. S3 in the ESI†), which agrees with the Φ value of generation of [Ru^{III}(Me$_2$phen)$_3$]$^{3+}$ without WOC ($vide$ $supra$).

Isotope-labelling experiments using ^{18}O^{18}O instead of ^{16}O^{16}O were conducted to obtain direct evidence for the
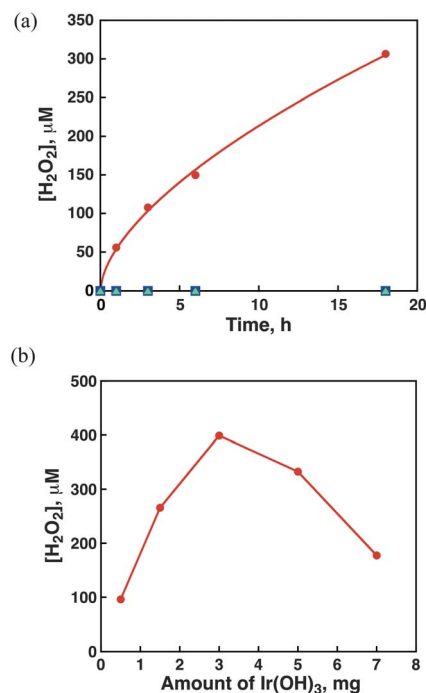
Fig. 5 (a) Time courses of H$_2$O$_2$ production under visible light (λ > 420 nm) irradiation of [Ru^{II}(Me$_2$phen)$_3$]$^{2+}$ (1.0 μM) in the presence of Ir(OH)$_3$ (3.0 mg) (red circles) and its absence (blue squares) in an O$_2$-saturated H$_2$SO$_4$ aqueous solution (2.0 M, 3.0 mL, [O$_2$] = 1.2 mM). A control experiment without [Ru^{II}(Me$_2$phen)$_3$]$^{2+}$ has been done in the presence of Ir(OH)$_3$ (3.0 mg) (green triangles). (b) Dependence of the amount of H$_2$O$_2$ produced after 1 h on the amounts of Ir(OH)$_3$ under visible light (λ > 420 nm) irradiation of [Ru^{II}(Me$_2$phen)$_3$]$^{2+}$ (20 μM) in an O$_2$-saturated H$_2$SO$_4$ aqueous solution.

3760 | *Energy Environ. Sci.*, 2013, **6**, 3756–3764

This journal is © The Royal Society of Chemistry 2013
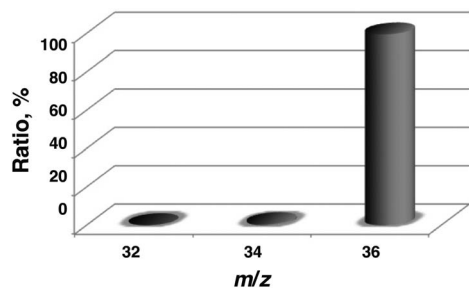
Fig. 6 Comparison of relative abundance of ^{18}O-labelled and unlabelled O_2, which was evolved by disproportionation of H_2O_2 produced in the photocatalytic reduction of $^{18}O^{18}O$ gas (≥98 at.%) containing $[Ru^{II}(Me_2phen)_3]^{2+}$ (20 μM) and $Ir(OH)_3$ (3.0 mg) in an $^{18}O_2$-saturated H_2SO_4 aqueous solution (2.0 M, 3.0 mL, $[O_2]$ = 1.2 mM) under photoirradiation (λ > 420 nm) for 1 h.

photocatalytic H_2O_2 production, in which the produced H_2O_2 comes from O_2 in the gas phase. After the reaction, the solution was carefully deaerated by bubbling with He gas to remove $^{18}O^{18}O$ and an excess of MnO_2, which catalysed the decomposition of H_2O_2 to O_2, was added to the solution. The evolved oxygen in the headspace of a reaction tube was separated using a gas chromatograph equipped with a molecular sieve column and analysed using a mass spectrometer (Fig. 6). Evolved O_2 was $^{18}O^{18}O$ (99%). There was no $^{16}O^{18}O$ or $^{16}O^{16}O$ incorporated from $H_2^{16}O$. This has confirmed that the produced H_2O_2 came from O_2 in the gas phase (not from water). The amount of evolved O_2 (0.76 mmol) in water oxidation reaction was only 0.71% as compared with the amount of introduced $^{18}O^{18}O$ (10^6 mmol). This is the reason why the evolution of O_2 containing ^{16}O from water was negligible.

3.3 Effect of Lewis acidity of metal ions on photocatalytic production of H_2O_2 from H_2O and O_2

The photocatalytic production of H_2O_2 was also examined using metal nitrates, $(M(NO_3)_n)$, acting as Lewis acids in water instead of H_2SO_4 under otherwise the same reaction conditions. The dependence of the photocatalytic reactivity of H_2O_2 production on the Lewis acidity of metal ions under the same pH
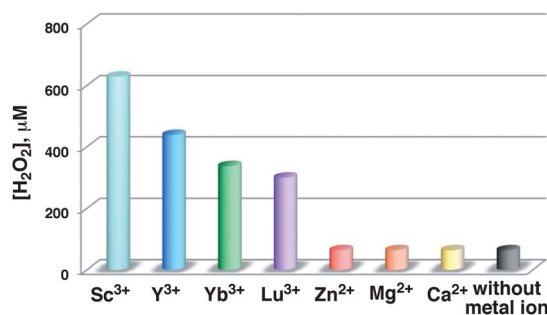
**Fig. 7** H_2O_2 production in the absence and presence of metal ions with Lewis acidity under irradiation of $[Ru^{II}(Me_2phen)_3]^{2+}$ (20 μM) with visible light (λ > 420 nm) for 1 h in the presence of $Ir(OH)_3$ (3.0 mg) and $M(NO_3)_n$ (M^{n+} = Sc^{3+}, Y^{3+}, Yb^{3+}, Lu^{3+}, Zn^{2+}, Mg^{2+} and Ca^{2+}, 100 mM) in O_2-saturated H_2O (3.0 mL, $[O_2]$ = 1.2 mM). The pH values of the solutions were adjusted to 2.8 by adding HNO_3.

conditions (pH 2.8) was examined as shown in Fig. 7, where $Sc(NO_3)_3$ exhibited the highest reactivity, which is in agreement with the strongest Lewis acidity of Sc^{3+}.[47–51] The Φ value of the photocatalytic H_2O_2 production in the presence of $Sc(NO_3)_3$ under visible light at λ = 450 nm was determined to be 12% (0–3 h, Fig. S4 in the ESI†).

The effect of $Sc(NO_3)_3$ on photoinduced electron transfer from $[Ru^{II}(Me_2phen)_3]^{2+*}$ to O_2 was examined by nanosecond laser flash photolysis measurements. The rate constants (k_{et}) of photoinduced electron transfer were determined by the emission quenching in the absence and presence of $Sc(NO_3)_3$ (Fig. S5 in the ESI†). The k_{et} values in both the absence and presence of $Sc(NO_3)_3$ are close to the diffusion-limited value (Table S3†). Thus, $Sc(NO_3)_3$ does not affect the oxidative quenching of $[Ru^{II}(Me_2phen)_3]^{2+*}$ by O_2.

The effect of $Sc(NO_3)_3$ on back electron transfer from O_2^{-} to $[Ru^{III}(Me_2phen)_3]^{3+}$ was examined by nanosecond laser flash photolysis measurements. The bleaching of absorption at λ = 445 nm due to $[Ru^{II}(Me_2phen)_3]^{2+}$ and the rapid recovery was observed in photoexcitation of $[Ru^{II}(Me_2phen)_3]^{2+}$ under O_2 due to back electron transfer from O_2^{-} to $[Ru^{III}(Me_2phen)_3]^{3+}$ (Fig. 8a). In the presence of Sc^{3+}, however, the recovery of absorption becomes significantly slower because of the binding of Sc^{3+} to O_2^{-}, which prohibits the back electron transfer (Fig. 8b). The slower recovery was also observed for other metal ions (Fig. 9).

Thus, the acceleration effect of $Sc(NO_3)_3$ on the photocatalytic production of H_2O_2 from H_2O and O_2 results from the inhibition of back electron transfer by binding of Sc^{3+} to O_2^{-}, which leads to more efficient generation of $[Ru^{III}(Me_2phen)_3]^{3+}$. In addition, the scandium ion inhibited disproportionation of H_2O_2 by $Ir(OH)_3$ under the same pH conditions as shown in Fig. 10.
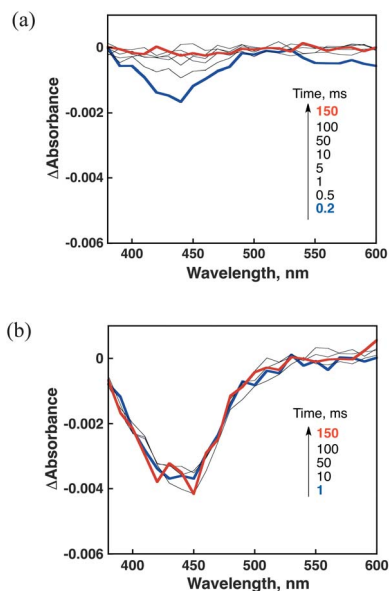

Fig. 8 Transient absorption spectra of $[Ru^{II}(Me_2phen)_3]^{2+}$ (20 μM) in O_2-saturated H_2O (a) in the absence of $Sc(NO_3)_3$ and (b) in the presence of $Sc(NO_3)_3$ (10 mM) after laser excitation at λ = 430 nm.

This journal is © The Royal Society of Chemistry 2013

Energy Environ. Sci., 2013, **6**, 3756–3764 | 3761
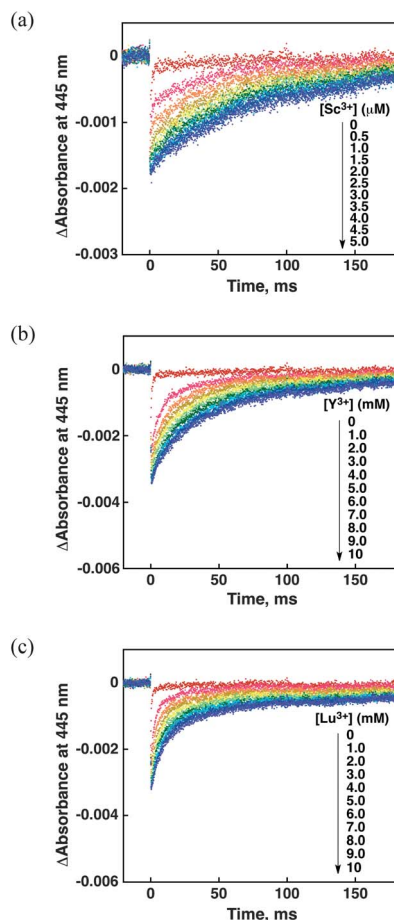
Fig. 9 Time profiles at $\lambda = 445$ nm for back electron transfer from $[Ru^{III}(Me_2\text{-}phen)_3]^{3+}$ to $O_2^{\cdot-}$ in O_2-saturated H_2O containing $[Ru^{II}(Me_2phen)_3]^{2+}$ (20 μM) in the presence of various concentrations of (a) $Sc(NO_3)_3$ (0–5.0 μM), (b) $Y(NO_3)_3$ (0–10 mM) and (c) $Lu(NO_3)_3$ (0–10 mM).

The formation of the $O_2^{\cdot-}$–Sc^{3+} complex during the photo-oxidation of $[Ru^{II}(Me_2phen)_3]^{2+}$ with O_2 in the presence of $Sc(NO_3)_3$ was confirmed by EPR measurements. When O_2-saturated H_2O of $[Ru^{II}(Me_2phen)_3]^{2+}$ in the presence of $Sc(NO_3)_3$
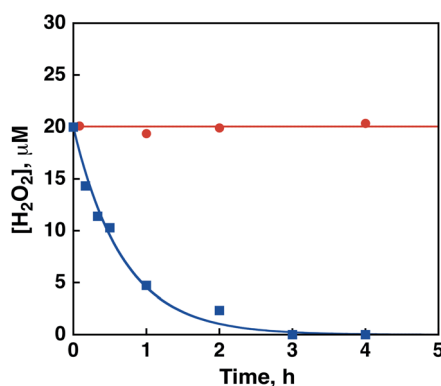
Fig. 10 Time courses of the concentration of H_2O_2 in the presence of $Ir(OH)_3$ (3.0 mg) in H_2O (3.0 mL) containing H_2O_2 (20 μM) and $Sc(NO_3)_3$ (100 mM) (red circles) at pH 2.8 and in an HNO_3 aqueous solution (pH 2.8, 3.0 mL) containing H_2O_2 (20 mM) (blue squares).
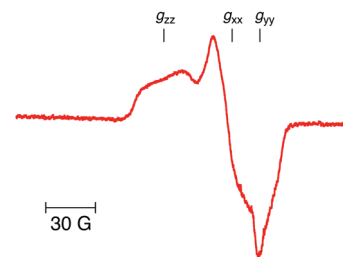
Fig. 11 EPR spectrum of the $O_2^{\cdot-}$–Sc^{3+} complex under irradiation of $[Ru^{II}(Me_2\text{-}phen)_3]^{2+}$ (20 μM) with visible light ($\lambda > 420$ nm) in the presence of $Sc(NO_3)_3$ (100 mM) in frozen O_2-saturated H_2O at 77 K.

was irradiated with visible light ($\lambda > 420$ nm), the $O_2^{\cdot-}$–Sc^{3+} complex was detected by the EPR spectrum in frozen H_2O at 77 K as shown in Fig. 11, where the superhyperfine structure due to the binding of Sc^{3+} ($I = 7/2$) was observed at g_{zz}. The g_{zz} value of $O_2^{\cdot-}$–Sc^{3+} (2.036) is larger than the value reported in frozen acetonitrile at 143 K (2.030),[47,52] because Sc^{3+} is easily hydrolysed in H_2O and the Lewis acidity of Sc^{3+} in H_2O is weaker than that in acetonitrile.[41]

3.4 Improvement of photocatalytic reactivity with a cobalt complex as WOC

The photocatalytic reactivity of H_2O_2 production was further improved by replacing $Ir(OH)_3$ nanoparticles by $[Co^{III}(Cp^*)(bpy)(H_2O)]^{2+}$.[36] The time courses of H_2O_2 production using $[Co^{III}(Cp^*)(bpy)(H_2O)]^{2+}$ as a WOC are shown in Fig. 12. The reactivity using $[Co^{III}(Cp^*)(bpy)(H_2O)]^{2+}$ is 4.3 times higher than that using $Ir(OH)_3$ at the initial stage (1 h). The TON based on $[Ru^{II}(Me_2phen)_3]^{2+}$ was determined to be 612 after 9 h photoirradiation.

After photoirradiation for 3 hours, the NMR peaks assignable to bpy and Cp^* still remained, indicating that $[Co^{III}(Cp^*)(bpy)(H_2O)]^{2+}$ remains as a homogeneous catalyst during the reaction (Fig. S6 in the ESI†). The photocatalytic reactivity increased with increasing the concentration of
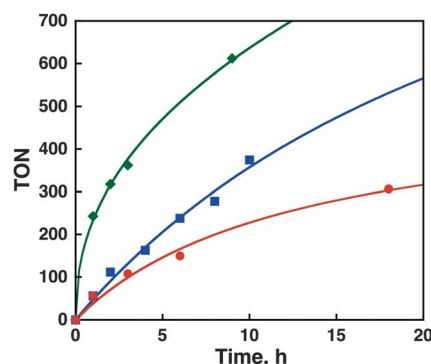
Fig. 12 Time courses of H_2O_2 production under visible light ($\lambda > 420$ nm) irradiation of $[Ru^{II}(Me_2phen)_3]^{2+}$ (1.0 μM) in the presence of $Ir(OH)_3$ (3.0 mg) in an O_2-saturated H_2SO_4 aqueous solution (2.0 M, 3.0 mL, $[O_2] = 1.2$ mM) (red circles), in the presence of $Ir(OH)_3$ (3.0 mg) and $Sc(NO_3)_3$ (100 mM) in O_2-saturated H_2O (3.0 mL, $[O_2] = 1.2$ mM) (blue squares), and in the presence of $[Co^{III}(Cp^*)(bpy)(H_2O)]^{2+}$ (10 mM) and $Sc(NO_3)_3$ (100 mM) in O_2-saturated H_2O (3.0 mL, $[O_2] = 1.2$ mM) (green diamonds).
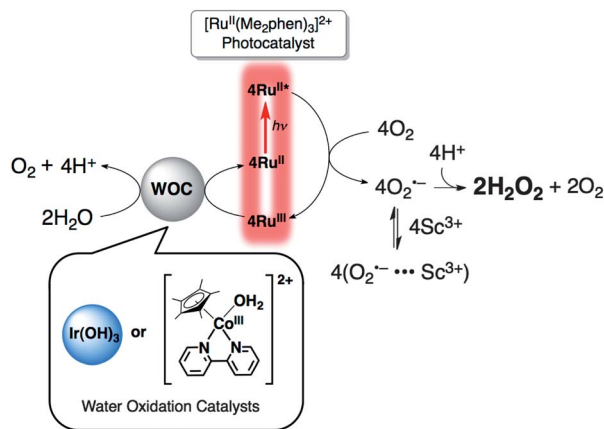
Scheme 1

$[Co^{III}(Cp^*)(bpy)(H_2O)]^{2+}$ (Fig. S7 in the ESI†). The concentration of $[Co^{III}(Cp^*)(bpy)(H_2O)]^{2+}$ is limited less than $ca.10$ mM because of the solubility.

The TON based on $[Co^{III}(Cp^*)(bpy)(H_2O)]^{2+}$ was determined to be 61 after 9 h photoirradiation. Thus, $[Ru^{II}(Me_2phen)_3]^{2+}$ and $[Co^{III}(Cp^*)(bpy)(H_2O)]^{2+}$ act as an efficient homogeneous photocatalyst and water oxidation catalyst, respectively. The Φ value of the photocatalytic H_2O_2 production under visible light irradiation at $\lambda = 450$ nm was determined using a ferrioxalate actinometer to be 37% (0–30 min, Fig. S8a in the ESI†). The value of conversion efficiency from solar energy to chemical energy was also determined to be 0.25% (0–10 min, Fig. S8b in the ESI†). This value has reached the solar energy conversion efficiency of switchgrass (0.2%),[53] a promising crop for biomass fuel.

In conclusion, efficient photocatalytic production of H_2O_2 from H_2O and O_2 has been achieved using $[Ru^{II}(Me_2phen)_3]^{2+}$ as a photocatalyst and $Ir(OH)_3$ nanoparticles or $[Co^{III}(Cp^*)-(bpy)(H_2O)]^{2+}$ as a WOC in water containing H_2SO_4 or $Sc(NO_3)_3$ as shown in Scheme 1. The photocatalytic production of H_2O_2 from H_2O and O_2 using solar energy reported in this paper provides the most convenient and sustainable solar fuel that can be converted to electricity using an H_2O_2 fuel cell. Further improvement of the catalytic reactivity and the more detailed elucidation of the catalytic mechanism are now in progress.

Acknowledgements

Notes and references

1 N. S. Lewis and D. G. Nocera, *Proc. Natl. Acad. Sci. U. S. A.*, 2006, **103**, 15729–15735.

2 D. G. Nocera, *Chem. Soc. Rev.*, 2009, **38**, 13–15.

3 H. B. Gray, *Nat. Chem.*, 2009, **1**, 7.

4 T. A. Faunce, W. Lubitz, A. W. Rutherford, D. MacFarlane, G. F. Moore, P. Yang, D. G. Nocera, T. A. Moore, D. H. Gregory, S. Fukuzumi, K. B. Yoon, F. A. Armstrong, M. R. Wasielewski and S. Styring, *Energy Environ. Sci.*, 2013, **6**, 695–698.

5 S. Fukuzumi, *Eur. J. Inorg. Chem.*, 2008, 1351–1362.

6 T. E. Mallouk, *J. Phys. Chem. Lett.*, 2010, **1**, 2738–2739.

7 B. Sorensen, *Hydrogen and fuel cells*, Elsevier Academic Press, London, UK, 2005.

8 *Hydrogen as a Future Energy Carrier*, ed. A. Zuttel, A. Borgschulte, L. Schlapbach, Wiley-VCH, Weinheim, 2008.

9 S. Fukuzumi, Y. Yamada, T. Suenobu, K. Ohkubo and H. Kotani, *Energy Environ. Sci.*, 2011, **4**, 2754–2766.

10 S. Fukuzumi and Y. Yamada, *J. Mater. Chem.*, 2012, **22**, 24284–24296.

11 K. Maeda, K. Teramura, D. L. Lu, T. Takata, N. Saito, Y. Inoue and K. Domen, *Nature*, 2006, **440**, 295–295.

12 A. Kudo and Y. Miseki, *Chem. Soc. Rev.*, 2009, **38**, 253–278.

13 K. Maeda, M. Higashi, D. Lu, R. Abe and K. Domen, *J. Am. Chem. Soc.*, 2010, **132**, 5858–5868.

14 X. B. Chen, S. H. Shen, L. J. Guo and S. S. Mao, *Chem. Rev.*, 2010, **110**, 6503–6570.

15 W. J. Youngblood, S. H. A. Lee, K. Maeda and T. E. Mallouk, *Acc. Chem. Res.*, 2009, **42**, 1966–1973.

16 Y. Tachibana, L. Vayssieres and J. R. Durrant, *Nat. Photon.*, 2012, **6**, 511–518.

17 M. K. Debe, *Nature*, 2012, **486**, 43–51.

18 S. Fukuzumi and T. Suenobu, *Dalton Trans.*, 2013, **42**, 18–28.

19 Y. Maenaka, T. Suenobu and S. Fukuzumi, *Energy Environ. Sci.*, 2012, **5**, 7360–7367.

20 R. S. Disselkamp, *Int. J. Hydrogen Energy*, 2010, **35**, 1049–1053.

21 A. E. Sanli and A. Aytac, *Int. J. Hydrogen Energy*, 2011, **36**, 869–875.

22 S. Fukuzumi, Y. Yamada and K. D. Karlin, *Electrochim. Acta*, 2012, **82**, 493–511.

23 Y. Yamada, Y. Fukunishi, S. Yamazaki and S. Fukuzumi, *Chem. Commun.*, 2010, **46**, 7334–7336.

24 Y. Yamada, S. Yoshida, T. Honda and S. Fukuzumi, *Energy Environ. Sci.*, 2011, **4**, 2822–2825.

25 S. A. M. Shaegh, N. T. Nguyen, S. M. M. Ehteshami and S. H. Chan, *Energy Environ. Sci.*, 2012, **5**, 8225–8228.

26 S. Yamazaki, Z. Siroma, H. Senoh, T. Loroi, N. Fujiwara and K. Yasuda, *J. Power Sources*, 2008, **178**, 20–25.

27 Y. Yamada, M. Yoneda and S. Fukuzumi, *Chem.–Eur. J.*, 2013, **19**, 11733–11741.

28 F. Sandelin, P. Oinas, T. Salmi, J. Paloniemi and H. Haario, *Ind. Eng. Chem. Res.*, 2006, **45**, 986–992.

29 S. Anandan and M. Miyauchi, *Chem. Commun.*, 2012, **48**, 4323–4325.

30 H. Kotani, K. Ohkubo and S. Fukuzumi, *Appl. Catal., B*, 2008, **77**, 317–324.

31 Y. Yamada, A. Nomura, T. Miyahigashi and S. Fukuzumi, *Chem. Commun.*, 2012, **48**, 8329–8331.

32 Y. Yamada, A. Nomura, T. Miyahigashi, K. Ohkubo and S. Fukuzumi, *J. Phys. Chem. A*, 2013, **117**, 3751–3760.

33 Y. Yamada, A. Nomura, K. Ohkubo, T. Suenobu and S. Fukuzumi, *Chem. Commun.*, 2013, **49**, 5132–5134.

34 D. Hong, M. Murakami, Y. Yamada and S. Fukuzumi, *Energy Environ. Sci.*, 2012, **5**, 5708–5716.

35 C. Turro, J. M. Zaleski, Y. M. Karabatsos and D. G. Nocera, *J. Am. Chem. Soc.*, 1996, **118**, 6060.

36 D. Hong, J. Jung, J. Park, Y. Yamada, T. Suenobu, Y. M. Lee, W. Nam and S. Fukuzumi, *Energy Environ. Sci.*, 2012, **5**, 7606–7616.

37 C. Turro, J. M. Zaleski, Y. M. Karabatsos and D. G. Nocera, *J. Am. Chem. Soc.*, 1996, **118**, 6060–6067.

38 C. Matsubara, N. Kawamoto and K. Takamura, *Analyst*, 1992, **117**, 1781–1784.

39 B. Saha and D. M. Stanbury, *Inorg. Chem.*, 2000, **39**, 1294–1300.

40 M. Hara, K. Asami, K. Hashimoto and T. Masumoto, *Electrochim. Acta*, 1983, **28**, 1073–1081.

41 H. Y. Hall and P. M. A. Sherwood, *J. Chem. Soc., Faraday Trans. 1*, 1984, **80**, 135–152.

42 G. Q. Wei, Y. X. Wang, C. D. Huang, Q. J. Gao, Z. T. Wang and L. Xu, *Int. J. Hydrogen Energy*, 2010, **35**, 3951–3957.

43 J. Yang, H. W. Liu, W. N. Martens and R. L. Frost, *J. Phys. Chem. C*, 2010, **114**, 111–119.

44 Y. Yamada, K. Yano, Q. A. Xu and S. Fukuzumi, *J. Phys. Chem. C*, 2010, **114**, 16456–16462.

45 A. Das, V. Joshi, D. Kotkar, V. S. Pathak, V. Swayambunathan, P. V. Kamat and P. K. Ghosh, *J. Phys. Chem. A*, 2001, **105**, 6945–6954.

46 C. T. Lin, W. Boettcher, M. Chou, C. Creutz and N. Sutin, *J. Am. Chem. Soc.*, 1976, **98**, 6536–6544.

47 S. Fukuzumi and K. Ohkubo, *Chem.–Eur. J.*, 2000, **6**, 4532–4535.

48 S. Fukuzumi and K. Ohkubo, *J. Am. Chem. Soc.*, 2002, **124**, 10270–10271.

49 K. Ohkubo, S. C. Menon, A. Orita, J. Otera and S. Fukuzumi, *J. Org. Chem.*, 2003, **68**, 4720–4726.

50 E. Y. Tsui, R. Tran, J. Yano and T. Agapie, *Nat. Chem.*, 2013, **5**, 293–299.

51 S. Fukuzumi, Y. Morimoto, H. Kotani, P. Naumov, Y.-M. Lee and W. Nam, *Nat. Chem.*, 2010, **2**, 756–759.

52 S. Fukuzumi, M. Patz, T. Suenobu, Y. Kuwahara and S. Itoh, *J. Am. Chem. Soc.*, 1999, **121**, 1605–1606.

53 A. Melis, *Plant Sci.*, 2009, **177**, 272–280.

3764 | *Energy Environ. Sci.*, 2013, **6**, 3756–3764

This journal is © The Royal Society of Chemistry 2013